Structural, optical, morphological and electrical properties of indium oxide thin films prepared by sol gel spin coating process

Article *in* Surface and Interface Analysis · December 2018

DOI: 10.1016/j.surfin.2018.12.012

CITATIONS
4

READS
712

8 authors, including:

Anouar Yahia
Université de Biskra
5 PUBLICATIONS **33** CITATIONS
SEE PROFILE

Abdallah Attaf
Université de Biskra
52 PUBLICATIONS **344** CITATIONS
SEE PROFILE

Hanane Saidi
Mohamed Khider University
42 PUBLICATIONS **211** CITATIONS
SEE PROFILE

Dahnoun Mohamed
Université de Biskra
6 PUBLICATIONS **33** CITATIONS
SEE PROFILE

Surfaces and Interfaces 14 (2019) 158–165

Contents lists available at ScienceDirect

Surfaces and Interfaces

journal homepage: www.elsevier.com/locate/surfin

Structural, optical, morphological and electrical properties of indium oxide thin films prepared by sol gel spin coating process

A. Yahia[a], A. Attaf[a,*], H. Saidi[a], M. Dahnoun[a], C. Khelifi[a], A. Bouhdjer[a], A. Saadi[a], H. Ezzaouia[b]

[a] Laboratoire de Physique des Couches Minces et Applications (LPCMA), University of Biskra, BP 145 RP, 07000 Biskra, Algeria
[b] Laboratoire des semi-conducteurs, nanostructures et Technologie Avancée, Research and Technology Centre of Energy, Borj-Cedria Science and Technology Park, BP 95, 2050 Hammam-Lif, Tunisia

ARTICLE INFO

Keywords:
In_2O_3 thin films
Sol gel
SEM
Optical properties
Photoluminescence
FTIR

ABSTRACT

Indium oxide (In_2O_3) thin films have been deposited by sol gel spin coating technique for different molar concentrations on glass substrates. X-ray diffraction spectra confirmed that the films have a polycrystalline nature with high preferred orientation along (222) plane corresponding to In_2O_3 cubic structure. Scanning electron microscope images show that the films have homogenous, uniform and dense surface without any pin holes and cracks. The Energy dispersive X-ray spectra confirm the presence of In and O elements in the deposited films. The optical analyses show that the films exhibit an optical transparency that reaches up to 90% in the visible range and optical band gap decreases from 4.04 to 3.88 eV. Photoluminescence spectra show mainly three emissions peaks (ultraviolet, blue and green), which decrease in the intensity with the raise of molar concentration. FTIR spectroscopy confirmed the presence of In–O and In–O–H absorption bands. Electrical measurements reveal that prepared films have a good conductivity (2.5×10^1 $(\Omega\ cm)^{-1}$).

1. Introduction

Indium oxide (In_2O_3) is very interesting semiconducting material exhibiting a wide band gap (> 3.5 eV), high transparency, considerable chemical stability, high mobility and electrical conductivity. It is commonly used for extent applications in the fields of electronic, photovoltaic and optoelectronic devices such as gas sensors [1], surface acoustic wave devices, light emitting diodes (LED) [2] and anti-reflecting coatings [3].

In_2O_3 thin films have been prepared by a variety of thin films deposition techniques such as pulsed laser deposition (PLD) [4], dc magnetron sputtering [5], spray pyrolysis [6], spray ultrasonic [7,8], sol gel process [9]. Of all the above techniques, the sol gel process has many merits compared to other well known methods such as; simplicity of the technique, the easy control of chemical components, low cost of the equipment, low temperature deposition and by this method we can produce high quality films with a variety of shapes and sizes. In the present work, In_2O_3 thin films were deposited by sol gel spin coating process on glass substrates by varying molar concentration from 0.05 to 0.25 M. The structural, surface morphological, optical and electrical properties of prepared In_2O_3 films were investigated in detail.

2. Experimental details

2.1. Preparation of In_2O_3 films

Indium oxide thin films were prepared by sol gel spin coating method using indium (III) nitrate hydrate [$In(NO_3)_3.xH_2O$], absolute ethanol (C_2H_6O) and acetylacetone ($C_5H_8O_2$) as precursor, solvent and stabilizer, respectively. The volume ratio of acetylacetone to ethanol was maintained at 1:10. Five different precursor concentrations from 0.05 to 0.25 M were prepared by taking different amounts of indium (III) nitrate hydrate into a fixed volume of ethanol. The solutions were then stirred for 2 h using a magnetic stirrer at 50 °C and they were aged for 48 h at room temperature. The prepared solutions were deposited on glass substrates and rotated for 30 s at 4000 rpm using a spin coater (bought from Holmarc) to get well coated films. To dry the films, the samples were placed in furnace for 10 min at 250 °C. The spin coating process was repeated six times to achieve the desired thickness. After that, the annealing process was carried out at 500 °C for 2 h to obtain good crystalline films.

The overall process used for the preparation of In_2O_3 thin films based on the sol gel spin coating process is shown in Fig. 1:

* Corresponding author.
E-mail address: ab_attaf@univ-biskra.dz (A. Attaf).

https://doi.org/10.1016/j.surfin.2018.12.012
Received 20 October 2018; Received in revised form 23 December 2018; Accepted 24 December 2018
Available online 25 December 2018
2468-0230/

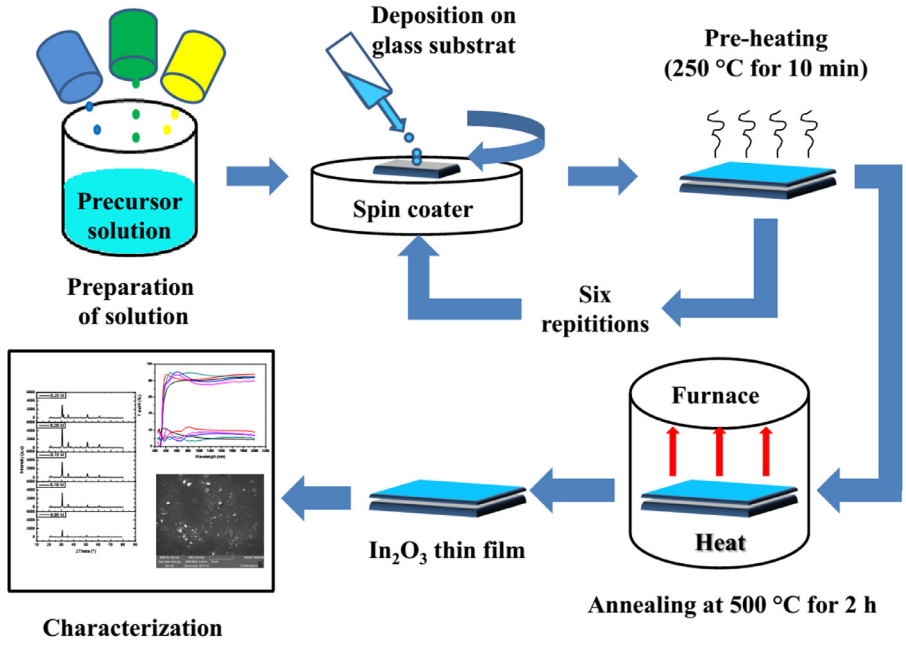

Fig. 1. Steps of thin film preparation in sol gel spin coating process.

2.3. Films characterization

The prepared films were characterized by an X-ray diffractometer (X'PERT PRO) to define the crystallite state and structural properties, scanning electron microscope (SEM) to analyze the surface morphology and energy dispersive X-ray (EDX) (attached to SEM) to evaluate films elemental composition. UV–visible spectrophotometer (Perkin Elmer LAMBDA 950 UV/VIS) to investigate the optical properties (gap energy, Urbach energy, refractive index, real and imaginary dielectric constant), fourier transform infrared (FTIR) spectrometer (BRUKER VERTEX-80 V) was used to obtain information about the chemical bonding in In_2O_3 films, photoluminescence (PL) spectrometer (Perkin Elmer LS 55) to detect luminescence regions and defect types. Four probe method to estimate the electrical conductivity (σ).

3. Results and discussion

3.1. Structural analysis

The XRD patterns of indium oxide thin films grown at different molar concentrations are illustrated in Fig. 2. As can be seen, all the films have a polycrystalline nature corresponding to cubic structure according to JCPDS card no. 06-0416 with preferential (222) peak. Films show other peaks corresponding to (211), (400), (440) and (622) planes. The growth along the (222) plane is due to the low free surface energy found in this direction for In_2O_3 cubic structure [10]. The increasing intensity of all peaks is attributed to the degree in crystalline state of the films. However, reduction in the intensity and appearance of new growth direction corresponds to (321) plane was observed for 0.25 M sample. This can be due to the deviation from cubic symmetry; which means that the composition (stoichiometry) of the In_2O_3 films is changing as a function of molar concentration.

Table 1 summarizes the structural parameters: Bragg's angle (2θ) and the inter-planar distance (d_{hkl}) for the predominant (222) peak. It has been observed that the calculated values of the inter-planar distance (d_{hkl}) were smaller than the standard values (JCPDS card 06-0416). This indicated that the crystalline cells submit to a compressive stress.

In order to calculate the crystallite size (D) and the strain (ε) of the films from the preferred orientation (222) plane at different molar concentrations, we have used the following equations [11,12]:

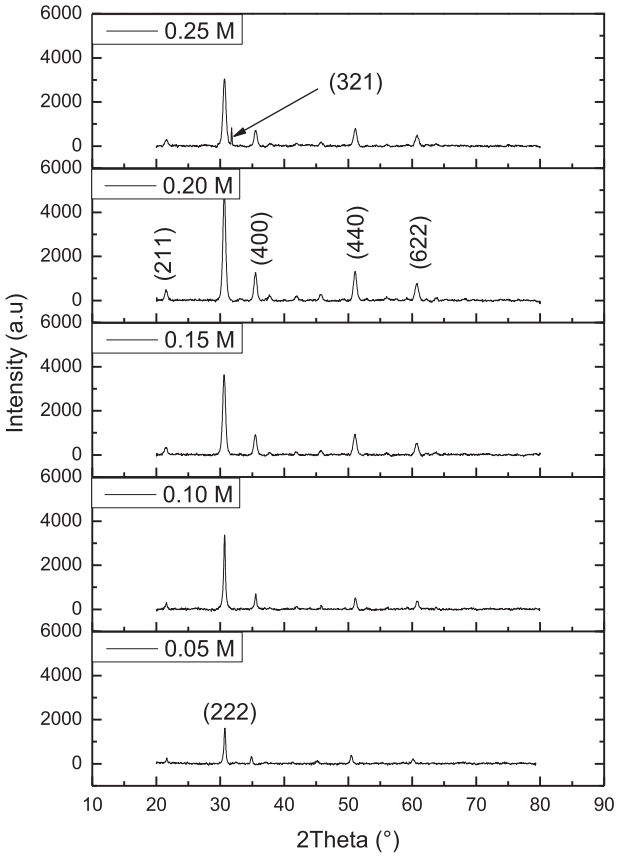

Fig. 2. XRD patterns of In_2O_3 thin films at different molar concentration.

$$D = \frac{K\lambda}{\beta cos\theta} \quad (1)$$

$$\varepsilon = \frac{\beta cos\theta}{4} \quad (2)$$

where D is the crystallite size, ε is the strain, K is a constant ($K = 0.9$), β is the full width at half maximum (FWHM), λ is X-ray wavelength

Table 1
The structural parameters of In_2O_3 films corresponding to (222) plane.

Preferred plane (hkl)	Molar concentration (M)	Standard 2θ (°)	The observed 2θ (°)	Standard d (Å)	The observed d_{hkl} (Å)	JCPDS card no.
	0.05		30.71		2.910	
	0.1		30.67		2.909	
(222)	0.15	30.58	30.60	2.921	2.920	06-0416
	0.2		30.63		2.917	
	0.25		30.65		2.910	

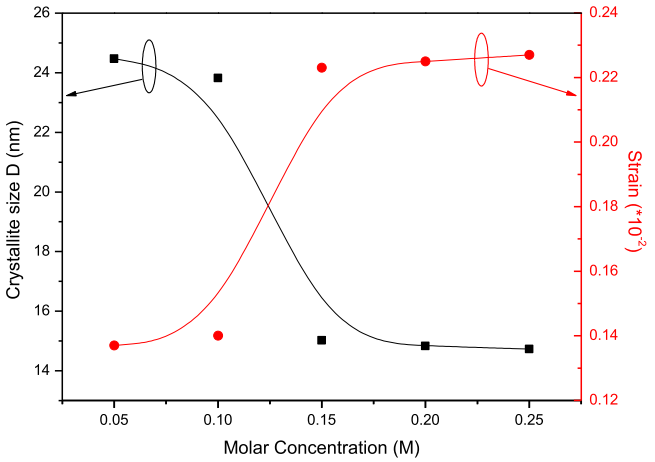

Fig. 3. Crystallite size and the strain as function of molar concentration.

($\lambda_{CuK\alpha}$ = 1.54060 Å) and θ is the angle of diffraction peak (Bragg's angle). The deconvolution of linewidth (β) was accomplished by Gaussian function [13]:

$$\beta = (\beta_{obs}^2 - \beta_m^2)^{1/2} \quad (3)$$

where β_{obs} is the measured peak width and β_m is the beak broadening due to the machine.

The crystallite size and the strain of In_2O_3 films grown at different molar concentrations are shown in Fig. 3. It is easy to note that the crystallite size and the strain have an opposite variation. The observed decrease in the crystallite size is commonly due to the augment in the internal strain [14]. Prathap et al. [15] reported that the decrease in crystallite size with increased molar concentration is attributed to the short time taken for the formation of crystallite.

The dislocation density (δ) is defined as the length of dislocations lines per unit of volume of the crystal and was estimated using Williamson and Smallman's relation [16]:

$$\delta = \frac{1}{D^2} \quad (4)$$

where D is the crystallite size. This equation is derived on the assumption that the material has a block structure similar to that found in microbeam studies and that the dislocations lie along the block surfaces [17].

The dislocation density of In_2O_3 films is illustrated in Fig. 4. As may be seen below, the dislocation density was about the range of 1.6×10^{15}–1.7×10^{15} line/m^2 at low molar concentrations, then it increased and stabilized about 4.6×10^{15} line/m^2 beyond 0.10 M. The increase in the dislocation density can be attributed to the decrease in crystallite size. Moreover, dislocations naturally become longer as dislocation lines extend to avoid micro-structural barriers that enhance by the decrease of crystallite size. May be that is the reason of the abrupt increase of dislocation density beyond 0.10 M. This result can be confirmed by the crystallite size variation.

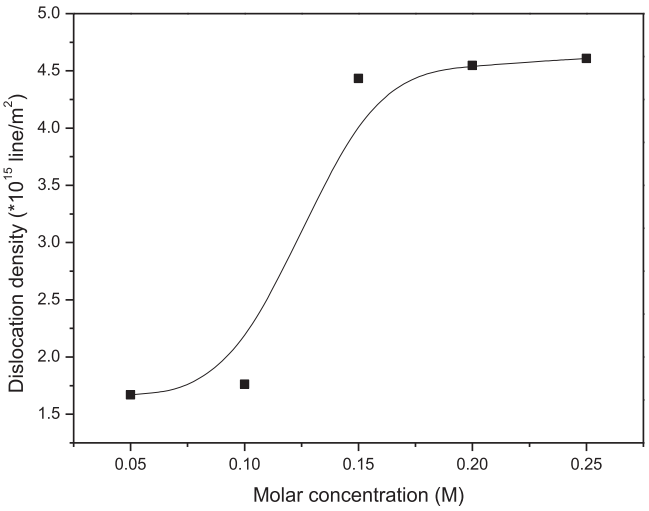

Fig. 4. The dislocation density of In_2O_3 films.

3.2. Surface morphological analysis

The surface morphology of films depends on the deposition technique, its parameters and it may influence mechanical, electrical and optical properties of the films. Fig. 5 shows the scanning electron micrographs of In_2O_3 films for different molar concentrations prepared by sol gel spin coating process. It is obvious that all the films have homogenous, uniform and dense surface without any pin holes and cracks. Moreover, the film deposited at 0.25 M show more roughness than the other films. The more roughness is probably due to a change in the surface structure of the film by the appearance of new growth in the [321] direction over the film surface, which was confirmed by XRD results.

The Energy dispersive X-ray (EDX) spectra of In_2O_3 films are shown in Fig. 6. As may be seen below, all EDX spectra reveal the presence of In and O elements in the deposited films. The peaks of other elements such as Si, Na, Mg and P are attributed to constituents of glass substrate. In addition, the EDX spectra also analyzed both of the weight percentage (w%) and atomic percentage (at%) of the indium and oxygen compounds. As can be seen, the weight percentage and atomic percentage of In and O elements vary with the precursor molar concentrations. It implies that the indium oxide compound could be In_2O_{3-x} (x could be positive or negative), this confirm the presence of oxygen vacancies.

3.3. Optical studies

Fig. 7 represents the transmittance (T) and reflectance (R) spectra of In_2O_3 thin films measured by Perkin Elmer LAMBDA 950 UV/VIS spectrophotometer in the wavelength range from 250 to 2000 nm. It is found that the In_2O_3 films deposited at different molar concentrations exhibit a high optical transparency about 80–90% in the visible range while the reflectance is found inside a confined interval 10–25%. Most of the samples show the presence of interference fringes in both reflectance and transmission spectra in the visible region; this can be

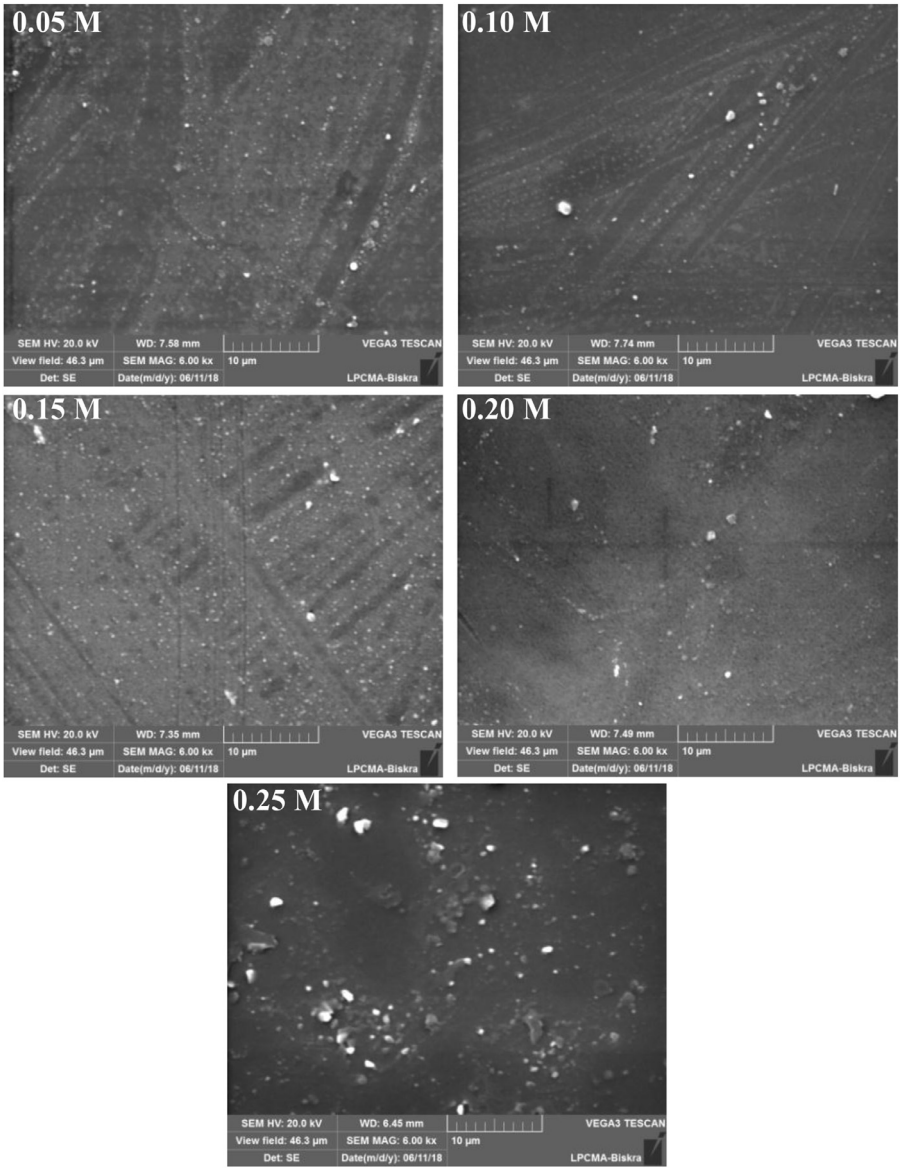

Fig. 5. Scanning electron microscopy images of prepared In_2O_3 thin films.

attributed to the homogenous and smooth surface of the films [18]. Furthermore, the transmittance spectra reveal a strong absorbance for all films in the range between 290 and 380 nm due to the excitation and the transition of electrons from the valence band (VB) to the conduction band (CB). This last phenomenon is very important characteristic for a semiconductor corresponding to the optical band gap energy (E_g).

Consider Fig. 8, which plots $(\alpha h\nu)^2$ against $h\nu$ for In_2O_3 films prepared at several precursor concentrations. The optical band gap (E_g) is determined by the extrapolation of the linear region of the curves to intersect at $h\nu$ axis following Tauc's formula [19]:

$$(\alpha h\nu) = A(h\nu - E_g)^m \tag{5}$$

where α is the absorption coefficient, $h\nu$ is the photon energy, A is an energy independent constant, E_g is the optical band gap energy and m assumes values of 1/2 and 2 for allowed direct, allowed indirect transitions, respectively. In our case, the value of m was selected to be 1/2 (for allowed direct band gap) as illustrated in Fig. 8, because we noticed a sudden steep rise (strong absorbance) for all films in transmittance spectra in the range of 290–380 nm.

The Urbach energy (E_u) is the band tail width and characterizes the disorder in film network, it is estimated from the plots of $Ln(\alpha)$ vs $h\nu$ (Fig. 9) by taken the inverse of the slope of the linear part using the following expressions [20]:

$$\alpha = \alpha_0 exp\left(\frac{h\nu}{E_u}\right) \tag{6}$$

$$E_u = \left[\frac{dLn(\alpha)}{dh\nu}\right]^{-1} \tag{7}$$

where α_0 is a constant and E_u is Urbach energy.

The variations of the optical band gap energy and Urbach energy of In_2O_3 films at different molar concentration are given in Fig. 10. From this figure it can be seen that the energy band gap was narrowing (from 4.04 to 3.88 eV) with increasing molar concentration. Whilst, Urbach energy changed inversely (increases from 249 to 285 meV). Increasing molar concentration causes an increase in the density of charges and then every electron is effectively surrounded by an exchange and correlating hole that lowers the energy level of the electrons, and the conduction band is shifted downwards [21]. Moreover, the calculated band gap of prepared In_2O_3 films is higher than that of In_2O_3 bulk. This is because of the quantum confinement effect due to small crystallite size of the polycrystalline In_2O_3 films [22].

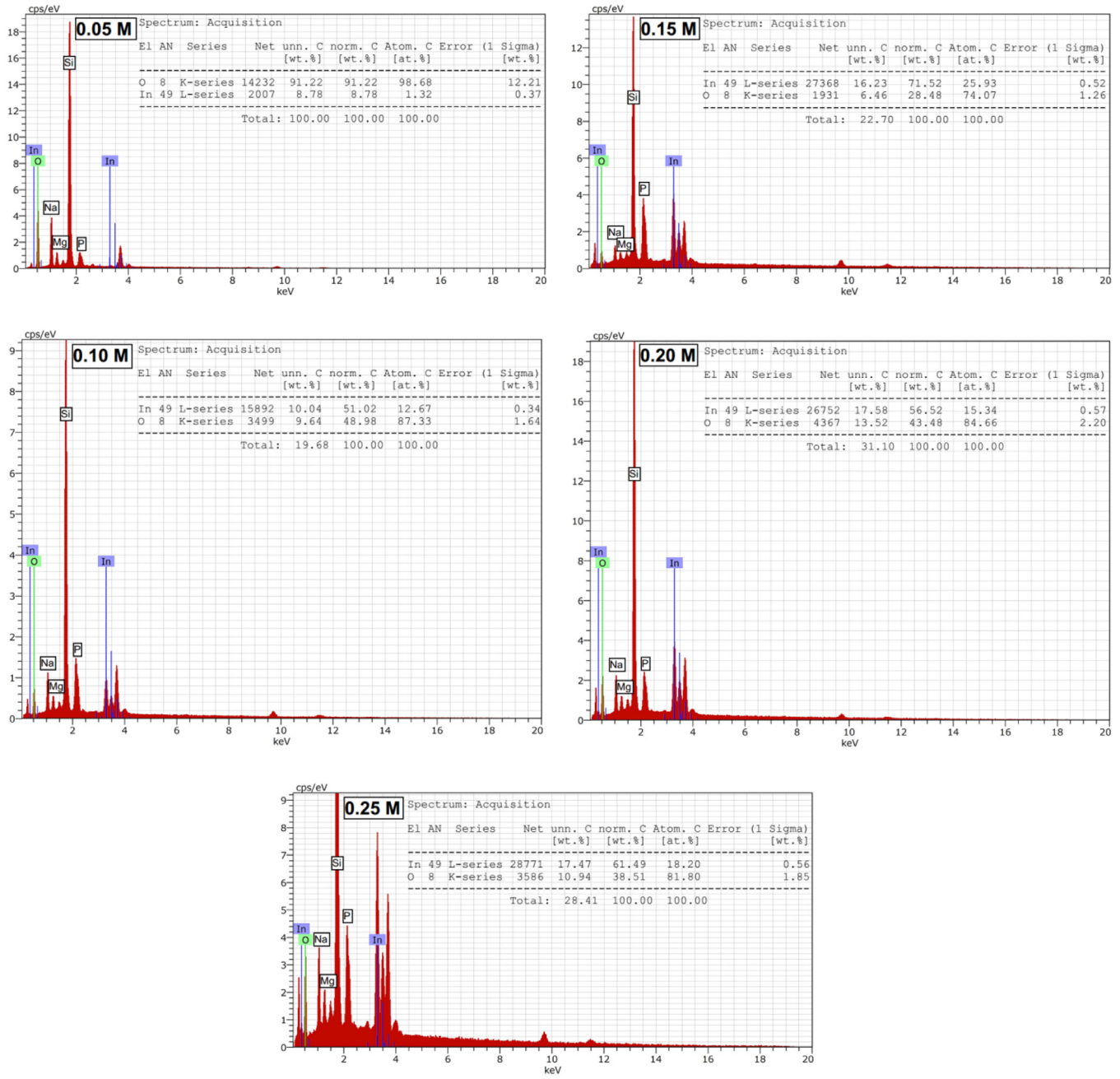

Fig. 6. Energy dispersive X-ray (EDX) spectra of In_2O_3 films.

The extinction coefficient (k) of In_2O_3 films is related to the absorption coefficient α through the following relation [23]:

$$k = \frac{\alpha\lambda}{4\pi} \tag{8}$$

where α is the absorption coefficient and λ is the wavelength.

The variation of extinction coefficient (k) with the wavelength (λ) for the grown films at various molar concentrations is shown in Fig. 11. As can be seen from Fig. 11 (inset), extinction coefficient shows high values that reach to 2.25 for 0.05 M in the low wavelengths (< 350 nm). Whilst, in the high wavelengths (> 350 nm), the extinction coefficient is very low (less than 0.25). The rise and the fall in the extinction coefficient (k) are directly related to the absorption of the light [24].

The refractive index (n) was determined from the reflectance (R) data using [25]:

$$n = \frac{(1+R)^{1/2}}{(1-R)^{1/2}} \tag{9}$$

The plots of refractive index (n) as function of the wavelength (λ) for In_2O_3 films deposited at different molar concentrations are given in Fig. 12. From these spectra it can be seen that n values of In_2O_3 films vary in the range of 1.7–2.9. All films show that the maximum of refractive index (n) is in the UV–visible region except the films deposited at 0.10 and 0.15 M, which had the maximum refractive index in the near IR region. Panneerdoss et al. [26] said that the maximum refractive index in the near IR region is possibly due to the stoichiometric form of the films.

The real (ε_1) and the imaginary (ε_2) parts of dielectric constant are determined by the relations bellow [27]:

$$\varepsilon_1 = n^2 - k^2 \tag{10}$$

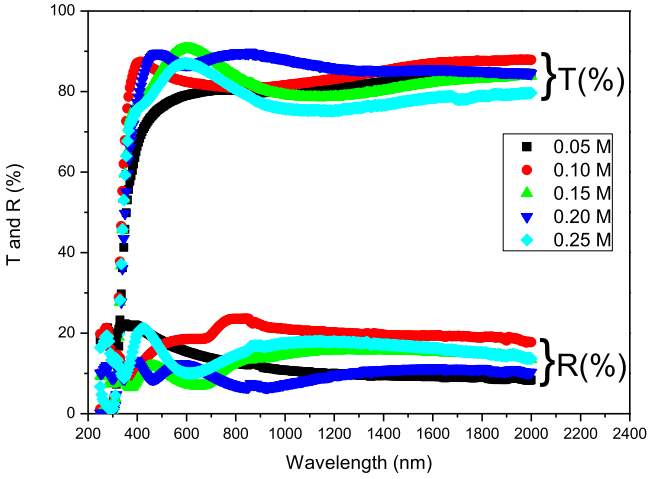

Fig. 7. The transmittance and reflectance spectra of In_2O_3 thin films.

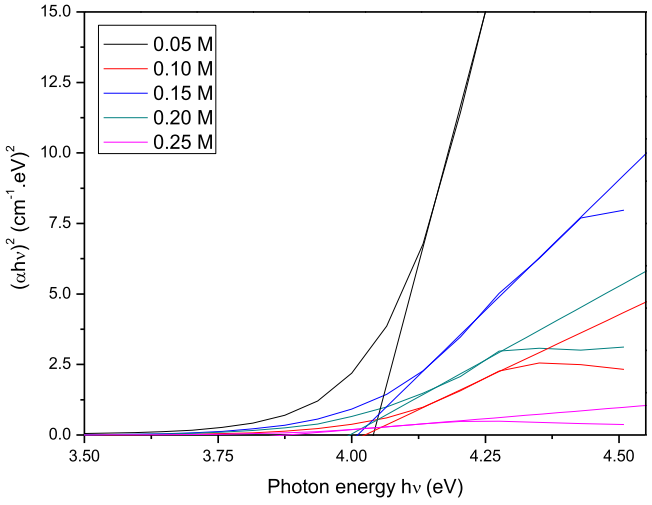

Fig. 8. Plots of $(\alpha h\nu)^2$ against hν of In_2O_3 films.

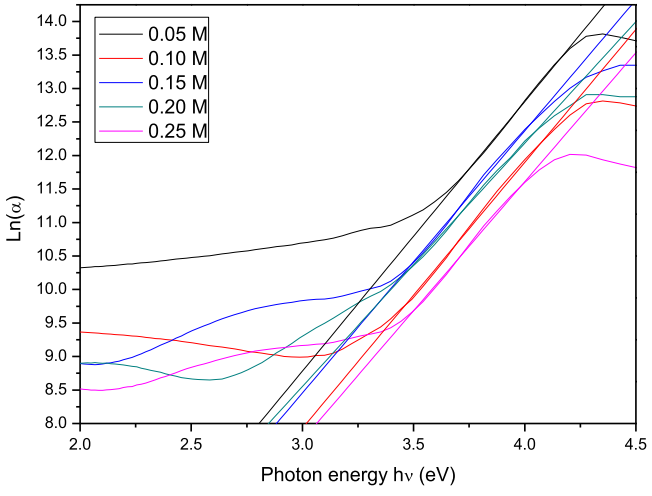

Fig. 9. Ln(α) vs hν plots of the films.

$$\varepsilon_2 = 2nk \tag{11}$$

where λ is the wavelength, ε_1 and ε_2 are the real and imaginary parts of the dielectric constant. Fig. 13 presents the variation of the real (ε_1) and imaginary (ε_2) parts of the dielectric constant with various molar concentrations. The values of ε_1 and ε_2 as function of wavelength are around of 1–8.5 and 0.8–12, respectively. Most studies reported that using low solution molar concentrations enhance the dielectric response of thin films due to the crystallite size modification, porosity and preferred orientation [28,29].

Fig. 14 shows the room temperature photoluminescence (PL) spectra of In_2O_3 films grown at various molar concentrations.

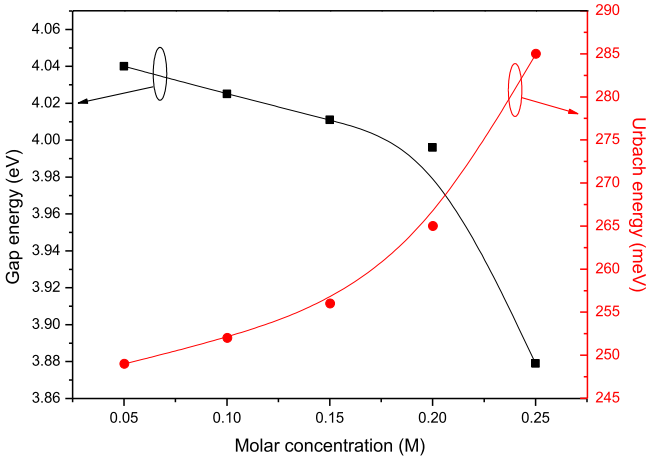

Fig. 10. Optical band gap and Urbach energy of In_2O_3 films.

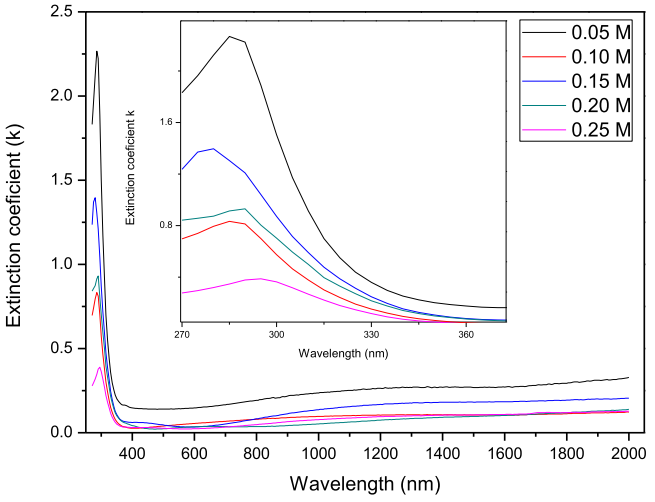

Fig. 11. Extinction coefficient as a function of wavelength for In_2O_3 films.

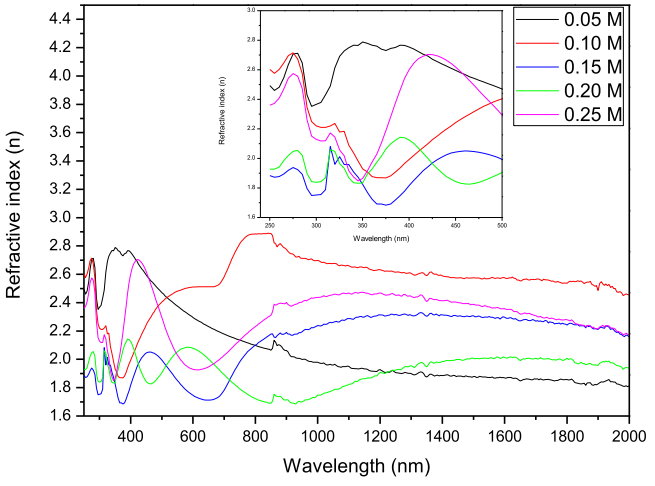

Fig. 12. The refractive index (n) of In_2O_3 films.

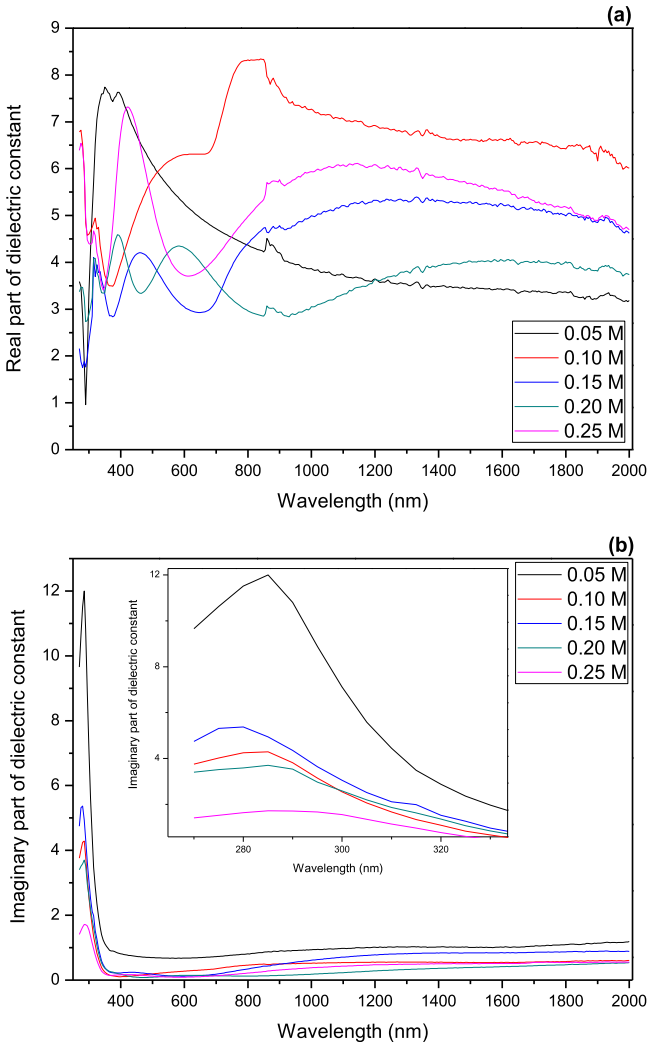

Fig. 13. The variation of: (a) the real and (b) the imaginary parts of dielectric constant.

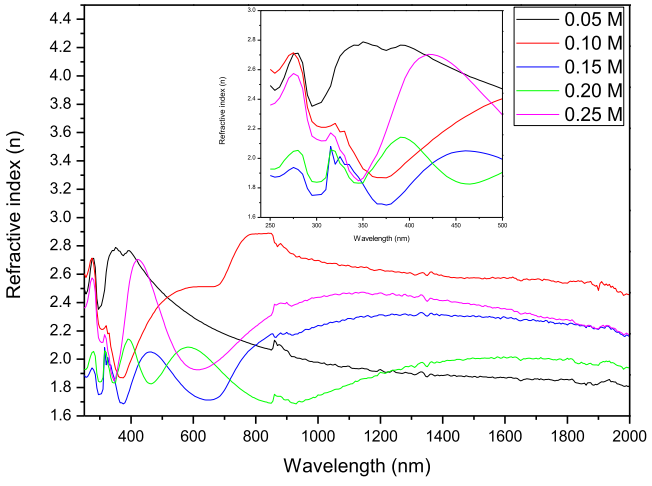

Fig. 14. PL spectra of indium oxide thin films at various molarities.

Photoluminescence spectra show mainly three emission peaks (ultraviolet, blue and green). The broad ultraviolet luminescence peak 310–420 nm is assigned to the near band edge (NBE) emission, which is attributed to the free exciton recombination between the conduction band (CB) and the valence band (VB) [30]. As shown in Fig. 14, a decrease observed in the broad ultraviolet emission peak could be due to the increased number of trap states in the mid-band gap region for non-radiative transition [31]. A blue emission band at 485 nm is referred to the new defect level that introduced into the band gap by the indium (In) atoms. The origin of green emission at 532 is generally ascribed to deep level defects such as surface defects and singly ionized oxygen vacancies [32].

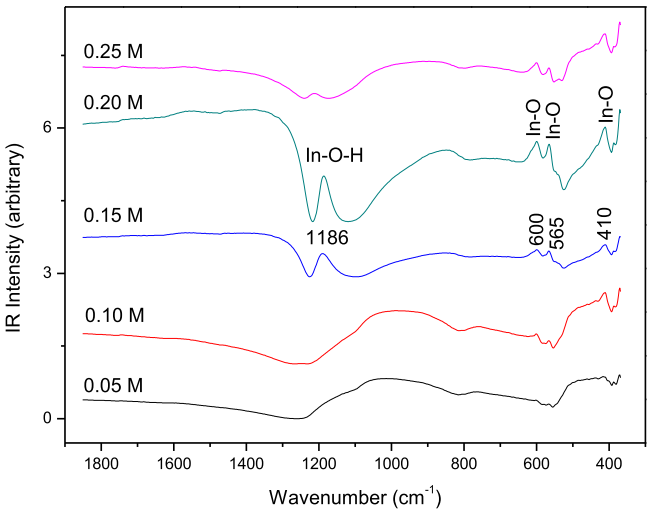

Fig. 15. FTIR spectra of In_2O_3 films at different molar concentrations.

FTIR technique is used to obtain information about the chemical bonding and the presence of certain functional groups in the films. The FTIR spectra of indium oxide films with various molar concentrations are shown in Fig. 15. The absorption bands shown by the films at 410, 565 and 600 cm^{-1} are referred to the In–O bond [33]. Return to the heavy mass of In atoms, the In–O stretching vibration modes are usually observed in the region of 800–300 cm^{-1}. We can also recognize absorption band at 1186 cm^{-1} related to In–O–H bending vibration [34]. It is obvious that the In–O and In–O–H absorption bands intensity increases with the increase of the molar concentration. This can be attributed to the enhancement of In atoms on the substrate surface which in turn leads to an increase in the probability of forming In–O and In–O–H bonds. However, the intensity of FTIR spectra reduced considerably for 0.25 M due to the degradation of the crystal state. These results are supported by the variation of XRD data.

3.4. Electrical studies

The electrical conductivity (σ) of indium oxide thin films was achieved using the following formula:

$$\sigma = \frac{1}{t}\left(\frac{ln2}{\pi}\frac{I}{U}\right) \tag{12}$$

where t is the film thickness, I is the current flowing through the outer tips of the probe and U is the voltage drop measured on the inner tips.

The conductivity of In_2O_3 films measured by four probe method at various molar concentrations can be found in Fig. 16. As can be seen, the electrical conductivity of In_2O_3 films increases from 0.58 to 2.5×10^1 $(\Omega\ cm)^{-1}$. The maximum conductivity value obtained in this work is 2.5×10^1 $(\Omega\ cm)^{-1}$ for the film deposited at 0.25 M. Many researchers claimed that the increase of the electrical conductivity is due to the enhancement of free carrier concentration [35]. In this work and in related references it was observed that the raise of electrical conductivity may be resulted from the interstitial indium atoms, which act as charge carrier donors to the conduction band.

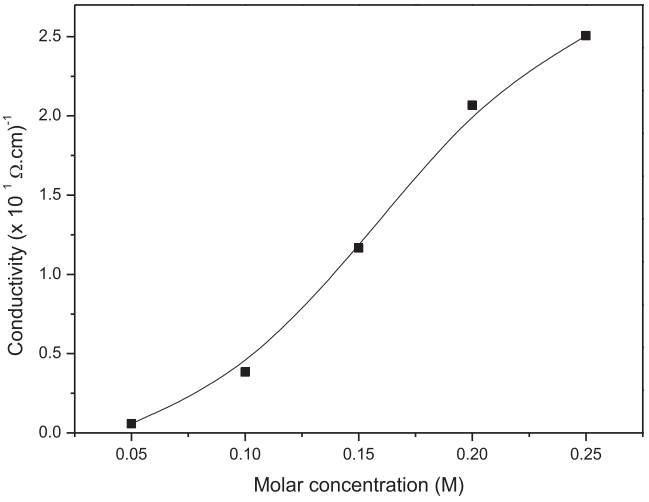

Fig. 16. Electrical conductivity as a function of molar concentration.

4. Conclusion

Indium oxide thin films with different molar concentrations have been successfully deposited by sol gel spin coating method on glass substrates. Effect of molar concentration on structural, morphological, optical and electrical properties was investigated. XRD patterns revealed that prepared films have a polycrystalline nature with strong orientation along (222) plane corresponding to In_2O_3 cubic structure. We observed an increase in the preferential growth in the (222) plane for films. Furthermore, we noticed emergence of new growth orientation for 0.25 M sample corresponding to (321) plane, which confirms the change in the composition (stoechiometry) at the film surface and the reduction of the preferential orientation. SEM images showed the homogenous and uniform distribution without any voids or cracks. The EDX spectra revealed the presence of In and O elements in the prepared films with their weight (w%) and atomic (at.%) percentage. Films exhibited a high optical transparency that reaches up to 90% in the visible range. In addition, we observed that the optical band gap energy (E_g) decreases from 4.04 to 3.88 eV. The decrease in PL peak intensity was indicating the increased number of trap states in the mid-band gap region for non-radiative transition. The presence of In–O and In–O–H absorption bands was confirmed by FTIR. Electrical measurements showed that molar concentration effectively increases the electrical conductivity from 0.58 to 2.5 × 10^1 $(\Omega\ cm)^{-1}$. From these findings, we conclude that the prepared In_2O_3 films can be used in optoelectronic applications such as buffer layer and transparent electrodes in solar cells. Also, the sol gel spin coating technique is suitable for producing homogenous and uniform thin films with good quality.

References

[1] S. Elouali, L.G. Bloor, R. Binions, I.P. Parkin, C.J. Carmalt, J.A. Darr, Gas sensing with nano-indium oxides (In_2O_3) prepared via continuous hydrothermal flow synthesis, Langmuir 28 (2012) 1879–1885.
[2] Y. Seki, S. Seki, Y. Hoshi, T. Uchida, Y. Sawada, Characteristics of vanadium-doped indium oxide thin films for organic light-emitting diodes fabricated by spray chemical vapor deposition, Jpn. J. Appl. Phys. 54 (2015) 041101.
[3] M. Girtan, H. Cachet, G.I. Rusu, On the physical properties of indium oxide thin films deposited by pyrosol in comparison with films deposited by pneumatic spray pyrolysis, Thin Solid Films 427 (2003) 406–410.
[4] J. Stankiewicz, X. Torrelles, J.L. García-Muñoz, J. Blasco, Structural and electrical properties of indium oxide thin films grown by pulsed laser deposition in oxygen ambient, J. Alloy. Compd. 694 (2017) 1280–1286.
[5] V. Binas, I. Kortidis, E. Gagaoudakis, K. Moschovis, G. Kiriakidis, Ageing resistant indium oxide ozone sensing films, Sens. Lett. 14 (2016) 563–566.
[6] A. Attaf, A. Bouhdjer, H. Saidi, M.S. Aida, N. Attaf, H. Ezzaouia, On tuning the preferential crystalline orientation of spray pyrolysis deposited indium oxide thin films, Thin Solid Films 625 (2017) 177–179.
[7] A. Bouhdjer, A. Attaf, H. Saidi, Y. Benkhetta, M.S. Aida, I. Bouhaf, A. Rhil, Influence of annealing temperature on In_2O_3 properties grown by an ultrasonic spray CVD process, Optik 127 (2016) 6329–6333.
[8] A. Bouhdjer, H. Saidi, A. Attaf, M.S. Aida, M. Jlassi, I. Bouhaf, H. Bendjedidi, Structural, morphological, optical, and electrical properties of In_2O_3 nanostructured thin films, Optik 127 (2016) 7319–7325.
[9] S. Ilican, M. Caglar, Y. Caglar, Structural, morphological and optical properties of indium oxide film by sol gel spin coating, J. Mater. Electron. Dev. 1 (2016) 19–23.
[10] A. Bouhdjer, A. Attaf, H. Saidi, H. Bendjedidi, Y. Benkhetta, I. Bouhaf, Correlation between the structural, morphological, optical, and electrical properties of In_2O_3 thin films obtained by an ultrasonic spray CVD process, J. Semicond. 36 (2015) 082002.
[11] A. Zolanvari, S. Hasansagha, F. Eshaghi, Z. Shahedi, A. Zendehnam, Microstructure and residual stress measurement of Ag/glass thin films using in-situ high-temperature X-ray diffraction, Armen. J. Phys. 9 (2016) 15–19.
[12] I. Bouhaf, Saidi Hanane, Attaf Abdallah, N. Attaf, R. Azizi, M. Jlassi, Influence of solution flow rate on the properties of SnS_2 films prepared by ultrasonic spray, Optik 127 (2016) 4043–4046.
[13] R. Delhez, T.H. De Keijser, E.J. Mittemeijer, Determination of crystallite size and lattice distortions through X-ray diffraction line profile analysis, Fresenius Z. Anal. Chem. 312 (1982) 1–16.
[14] B.G. Jeyaprakash, R.A. Kumar, K. Kesavan, A. Amalarani, Structural and optical characterization of spray deposited SnS thin film, J. Am. Sci. 6 (2010) 22–26.
[15] P. Prathap, Y.P.V. Subbaiah, K.R. Reddy, Effect of precursor molarity on physical properties of In_2O_3 films, Optoelectron, Adv. Mater. Rapid Commun. 1 (2007) 252–260.
[16] S. Chander, M.S. Dhaka, Preparation and physical characterization of CdTe thin films deposited by vacuum evaporation for photovoltaic applications, Adv. Mater. Lett. 6 (2015) 907–912.
[17] G.K. Williamson, R.E. Smallman, III. Dislocation densities in some annealed and cold-worked metals from measurements on the X-ray debye-scherrer spectrum, Philos. Mag. 1 (1956) 34–46.
[18] X.Y. Li, H.J. Li, Z.J. Wang, H. Xia, Z.Y. Xiong, J.X. Wang, B.C. Yang, Effect of substrate temperature on the structural and optical properties of ZnO and Al-doped ZnO thin films prepared by dc magnetron sputtering, Opt. Commun. 282 (2009) 247–252.
[19] L. Chen, J. Deng, H. Gao, Q. Yang, L. Kong, M. Cui, Z. Zhang, Ellipsometric study and application of rubrene thin film in organic Schottky diode, Appl. Surf. Sci. 388 (2016) 396–400.
[20] T.P. Rao, M.C. Santhosh, Physical properties of Ga doped ZnO thin films by spray pyrolysis, J. Alloy. Compd. 506 (2010) 788–793.
[21] A.I.A. Ali, Molarities effect on structural and optical properties of ZnO prepared by spray pyrolysis, IJSER 5 (2014) 2250–2256.
[22] M.P. Sarma, G. Wary, Effect of molarity on structural and optical properties of chemically deposited nanocrystalline PbS thin film, ILCPA 74 (2017) 22–35.
[23] N. Fellahi, M. Addou, A. Kachouane, M. El Jouad, Z. Sofiani, Optical properties of undoped and tin-doped nanostructured In_2O_3 thin films deposited by spray pyrolysis, Eur. Phys. J. Appl. Phys. 74 (2016) 24611.
[24] M. Jothibas, C. Manoharan, S. Dhanapandian, S.J. Jeyakumar, Influence of precursor concentration on sprayed In_2O_3 thin films, Asian J. Chem. 25 (2013) S59–S64.
[25] C. Manoharan, M. Jothibas, S.J. Jeyakumar, S. Dhanapandian, Structural, optical and electrical properties of Zr-doped In_2O_3 thin films, Spectrochim. Acta Mol. Biomol. Spectrosc. 145 (2015) 47–53.
[26] I.J. Panneerdoss, S.J. Jeyakumar, S. Ramalingam, M. Jothibas, Characterization of prepared In_2O_3 thin films: The FT-IR, FT-Raman, UV–visible investigation and optical analysis, Spectrochim. Acta A 147 (2015) 1–13.
[27] F. Yakuphanoglu, S. Ilican, M. Caglar, Y. Caglar, The determination of the optical band and optical constants of non-crystalline and crystalline ZnO thin films deposited by spray pyrolysis, J. Optoelectron. Adv. Mater. 9 (2007) 2180–2185.
[28] C.V. Weiss, M.W. Cole, S.P. Alpay, Influence of the precursor solution molarity on the dielectric response of chemical solution deposited strontium titanate thin films on Si, Integr. Ferroelectr 126 (2011) 7–16.
[29] Z. Jiwei, Y. Xi, Z. Liangying, S. Bo, H. Chen, Orientation control and dielectric properties of sol–gel deposited Ba (Ti, Zr)O_3 thin films, J. Cryst. Growth 262 (2004) 341–347.
[30] T.V. Vimalkumar, N. Poornima, C.S. Kartha, K.P. Vijayakumar, Effect of precursor medium on structural, electrical and optical properties of sprayed polycrystalline ZnO thin films, Mater. Sci. Eng. B 175 (2010) 29–35.
[31] P. Babu, K.R. Reddy, R.W. Miles, Precursor concentration effect on the properties of $ZnIn_2Se_4$ layers grown by chemical bath deposition, Energy Procedia 10 (2011) 177–181.
[32] Y. Li, Y. Bando, D. Golberg, Single-crystalline In_2O_3 nanotubes filled with, Adv. Mater. 15 (2003) 581–585.
[33] M. Jothibas, C. Manoharan, S. Ramalingam, S. Dhanapandian, S.J. Jeyakumar, M. Bououdina, Preparation, characterization, spectroscopic (FT-IR, FT-Raman, UV and visible) studies, optical properties and Kubo gap analysis of In_2O_3 thin films, J. Mol. Struct. 1049 (2013) 239–249.
[34] M.I. Ivanovskaya, E.A. Ovodok, D.A. Kotsikau, Sol–Gel synthesis and features of the structure of Au–In_2O_3 nanocomposites, Glass Phys. Chem. 37 (2011) 560–567.
[35] M. Ghougali, O. Belahssen, A. Chala, Structural, optical and electrical properties of NiO nanostructure thin film, J. Nano-Electron. Phys. 8 (2016) 04059.